

# On the Correction of Partial Beam Blockage in Polarimetric Radar Data

TIMOTHY J. LANG

*Department of Atmospheric Science, Colorado State University, Fort Collins, Colorado*

STEPHEN W. NESBITT

*Department of Atmospheric Sciences, University of Illinois at Urbana–Champaign, Urbana, Illinois*

LAWRENCE D. CAREY

*Earth System Sciences Center, National Space Science and Technology Center, University of Alabama in Huntsville, Huntsville, Alabama*

(Manuscript received 10 March 2008, in final form 2 October 2008)

## ABSTRACT

Three methodologies for correcting the radar reflectivity factor ( $Z_H$ ) in the presence of partial beam blockage are implemented, compared, and evaluated using a polarimetric radar dataset from the North American Monsoon Experiment (NAME) in northwestern Mexico. One methodology uses simulated interactions between radar beams and digital terrain maps, while the other two invoke the self-consistency of polarimetric radar measurands in rainfall, and the relative insensitivity of a specific differential phase to beam blockage. While the different methodologies often agree to within 1–2 dB, significant disagreements can occur in regions of sharp azimuthal gradients in beam blockage patterns, and in areas where the terrain-caused radar clutter map is complex. These disagreements may be mitigated by the use of additional radar data to develop the polarimetric correction techniques, by a more sophisticated terrain-beam interaction model, or by a higher-resolution digital terrain map. Intercomparisons between ground radar data and Tropical Rainfall Measuring Mission satellite overpasses suggest that all of the methodologies can correct mean  $Z_H$  to within the expected uncertainty of such intercomparisons (1–1.5 dB). The polarimetric correction methods showed good results even in severely blocked regions (>10 dB reduction). The results suggest the possibility that all of the techniques may be valid approaches to correcting partial beam blockage, and within that context relative advantages and disadvantages of each technique are discussed. However, none of the techniques can correct radar data when weak echoes are reduced to noise by strong blocks, thus leading to biases in corrected  $Z_H$  and rainfall climatologies.

## 1. Introduction

### *a. Background*

Partial beam blockage (PBB) can be a major concern when using radar data, especially when the radar is in a region of complex terrain. Beyond creating ground clutter echo, the interception of low-elevation angle radar beams by the intervening terrain causes a low bias in radar reflectivity ( $Z$ ) measurements behind blocking terrain, and even can lead to the total loss of signal in

extreme cases (e.g., Germann and Joss 2003). Effects on subsequent rainfall estimation, via reflectivity–rainfall ( $Z$ – $R$ ) relationships, can be drastic as even a 3-dB loss in signal halves the reflectivity estimate (in  $\text{mm}^6 \text{m}^{-3}$ ) used in any  $Z$ – $R$  relationship, thus introducing large negative biases in the estimated precipitation rate. Given the desire to produce the best radar quantitative precipitation estimates in complex terrain, beam blockage correction offers the potential to extend quantitative rainfall estimates over broader regions in mountainous areas, which is important in regions prone to flash flooding. In addition, studies of the spatial distribution and microphysical structure of orographic precipitation in complex terrain would benefit from accurate low-level reflectivity (and estimated rain rate) distributions.

---

*Corresponding author address:* Timothy J. Lang, Dept. of Atmospheric Science, Colorado State University, Fort Collins, CO 80523.

E-mail: tlang@atmos.colostate.edu

Past studies of PBB with conventional single-polarization radars have used digital elevation models (DEMs) as their cornerstone. The DEMs can be used in different ways. Many studies use DEMs to identify blocked rays, and the reflectivity correction is based on the vertical profile of  $Z$  (VPR) using data from higher-elevation angles (e.g., Andrieu et al. 1997; Creutin et al. 1997; Dinku et al. 2002; Kucera et al. 2004). Other studies estimate the percentage of beam blockage using radar beam geometry calculations and DEMs (e.g., Bech et al. 2003). They may then use long-term rain gauge and VPR estimates to refine the corrections. Examples of the latter methodology include operational radar blockage correction schemes in Switzerland and France (Germann et al. 2006; Tabary 2007; Tabary et al. 2007).

Recently, methodologies for correcting PBB using polarimetric radar data have been introduced (Carey et al. 2000; Cifelli et al. 2002; Giangrande and Ryzhkov 2005). These methods are based on the relative insensitivity of a specific differential phase ( $K_{DP}$ ) to PBB. Indeed, the power signal just has to be sufficiently above noise to use  $K_{DP}$  without impact (Ryzhkov and Zrnić 1996; Zrnić and Ryzhkov 1996; Vivekanandan et al. 1999; Friedrich et al. 2007).

The Carey et al. (2000) and Cifelli et al. (2002) methodologies depend upon the self-consistency of polarimetric variables in rainfall (Goddard et al. 1994; Scarchilli et al. 1996; Ryzhkov et al. 2005). It corrects horizontal reflectivity ( $Z_H$ ) by utilizing radar data in unblocked azimuths to generate an empirical self-consistent relation between  $Z_H$  and  $K_{DP}$ . For a specified range of  $K_{DP}$ , a fixed range of  $Z_H$  is expected in rain (Balakrishnan and Zrnić 1990). The narrower the range of  $K_{DP}$  used, the less drop size distribution (DSD)—and thus  $Z_H$ —variability is expected. The azimuthal trend in this  $Z_H$  range is investigated, with unblocked azimuths compared against blocked ones. The observed average  $Z_H$  difference between a specific blocked azimuth, and a collection of unblocked azimuths, is used to increase all observed  $Z_H$  values at that azimuth. While the methodology has been used to develop realistic corrections to  $Z_H$  (Cifelli et al. 2002; Lang et al. 2007), it has undergone limited verification or comparison against other PBB correction methodologies.

The correction methodology of Giangrande and Ryzhkov (2005) also is based on the self-consistency of polarimetric measurands in rainfall, but includes differential reflectivity ( $Z_{DR}$ ) in addition to  $Z_H$  and  $K_{DP}$ . Giangrande and Ryzhkov (2005) first corrected PBB in  $Z_{DR}$  by examining the mean azimuthal variability of  $Z_{DR}$  in light rain or snow. Polarimetrically based hydrometeor identification and  $K_{DP}$  (if examining light rain) are used to partition the data in order to ensure the

correct hydrometeor species and precipitation rate. PBB is identified and quantified by examining the mean bias in  $Z_{DR}$  between a particular blocked azimuth and unblocked ones, similar to how Carey et al. (2000) and Cifelli et al. (2002) correct  $Z_H$ . Then,  $Z_H$  is corrected using area–time integrals of polarimetric variables and self-consistency functions of the form  $Z_H = f(Z_{DR}, K_{DP})$ . Self-consistency functions are dependent on assumptions regarding the drop size distribution and the drop shape versus size relation (Ryzhkov et al. 2005). Giangrande and Ryzhkov (2005) found that their methodology could correct  $Z_{DR}$  to within 0.2–0.3 dB, while  $Z_H$  could be corrected to within 2–3 dB.

#### *b. The problem of limited radar deployments in poorly understood mountainous regions*

During the North American Monsoon Experiment (NAME; Higgins et al. 2006) field campaign, the National Center for Atmospheric Research (NCAR) S-band dual-polarization Doppler radar (S-Pol) was stationed for ~6 weeks along the Gulf of California coast, in full view of the Sierra Madre Occidental (SMO) to the east. The dataset was severely affected by PBB (Fig. 1; see also Lang et al. 2007). Unlike many operational radar networks in mountainous regions, such as those in Europe (e.g., Germann et al. 2006; Tabary 2007), there was limited rain gauge support for the S-Pol radar. Despite the extensive NAME Event Rain Gauge Network (Gochis et al. 2007), the closest gauge to S-Pol was over 40 km away, in an unblocked sector. The next closest gauge was ~90 km away. Thus, given the short time frame for the experiment, and the sparse distribution of gauges close to the radar, there was limited ability to use rain gauge data to refine or validate any PBB correction scheme applied to this dataset.

Furthermore, in this region, fundamental scientific uncertainties exist about variability in the vertical structure of precipitating systems and in DSDs and drop shape as functions of terrain (Nesbitt et al. 2008; Rowe et al. 2008). Therefore, the application of VPR-based corrections (e.g., Joss and Lee 1995; Pellarin et al. 2002), or DSD- and drop-shape-dependent corrections using polarimetric self-consistency functions, as in Giangrande and Ryzhkov (2005), may be problematic.

Given these limitations, it is not immediately clear which PBB-correction methodology would be best for datasets like NAME and other blockage-affected field projects, such as the recently completed Terrain-influenced Monsoon Rainfall Experiment (TiMREX) in Taiwan. In this paper, using the NAME radar dataset, two polarimetric PBB-correction methodologies will be compared against a simple DEM-based methodology, and both will be compared against the well-calibrated Tropical Rainfall

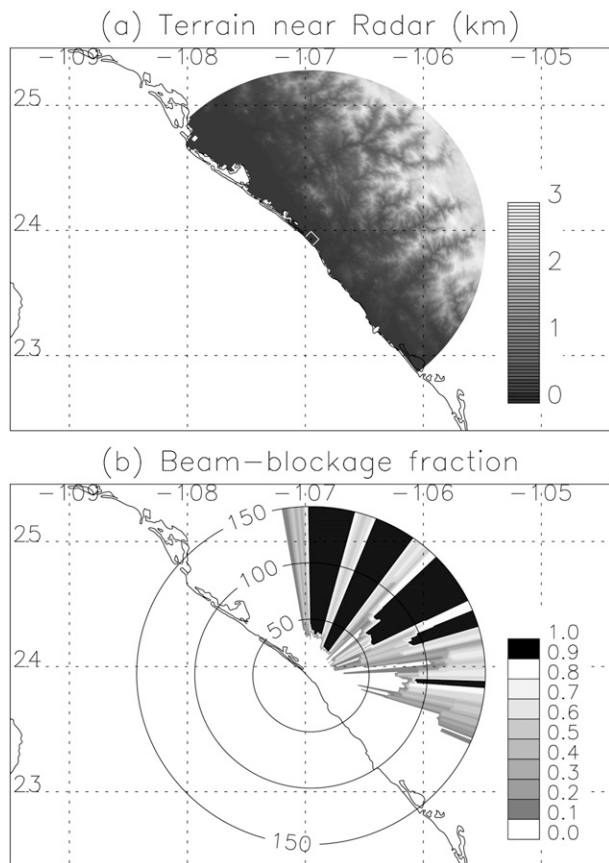


FIG. 1. (a) Terrain within 150 km of S-Pol during NAME 2004. (b) Estimated S-Pol beam-blockage fraction during NAME.

Measuring Mission precipitation radar (TRMM PR; Simpson et al. 1988; Anagnostou et al. 2001) reflectivity data. Relative strengths and weaknesses of the methodologies will be assessed. Section 2 briefly outlines the radar data along with the polarimetric and DEM methodologies. Results and conclusions are presented in sections 3 and 4, respectively

## 2. Data and methodology

### a. S-Pol radar

The NCAR S-Pol radar is an S-band dual-linearly polarized Doppler radar. During NAME it was deployed from 8 July through 21 August 2004 along the coast of the Gulf of California (Fig. 1a). S-Pol primarily scanned multitilt, full 360° azimuth volumes in plan position indicator (PPI) format, with an update cycle of 15 min. The proximity of the SMO led to an extremely large amount of blockage over much of S-Pol's land coverage. This blockage persisted in some form up to 2.0° elevation. Prior to any blockage correction, the S-Pol dataset was subject to significant polarimetric-

based quality control to eliminate clutter, insects, second-trip and other spurious echoes, and to correct both  $Z_H$  and  $Z_{DR}$  for attenuation by gases and rainfall, as detailed in Lang et al. (2007; information online at [http://data.eol.ucar.edu/datafile/nph-get/82.119/readme\\_NAME\\_regional\\_radar\\_composites\\_v2.1.pdf](http://data.eol.ucar.edu/datafile/nph-get/82.119/readme_NAME_regional_radar_composites_v2.1.pdf)). While the methodology descriptions below focus mainly on 0.8° elevation sweeps, all of the correction techniques also were applied to higher tilts (i.e., 1.3° and 1.8°) for the TRMM PR intercomparison in section 3.

### b. DEM method

The DEM-based PBB correction method (hereafter referred to as the DEM method) was based on equations used by Battan (1973) to describe beam propagation in a standard atmosphere (i.e., the 4/3 earth radius approximation). Once the propagation characteristics of the beam were calculated, topography was matched to the simulated range bins of the radar. The topography was given by the 30-arcsec-resolution U.S. Geological Survey GTOPO-30 DEM (information online at <http://eros.usgs.gov/products/elevation/gtopo30/gtopo30.html>). The DEM was linearly interpolated to a polar coordinate system (the S-Pol radar site constituting the origin) with 250-m radial spacing and 1° azimuth spacing, taking into account the effective loss of distance along the ground caused by the beam's height gain along the radial. The methodology of Bech et al. (2003) then was used to calculate a beam blockage fraction at each azimuth and range gate. The method considers the intersection of a 1° Gaussian main lobe with the DEM terrain and calculates the fraction of the beam's power that is blocked (beam blockage fraction).

An example of the simulated beam blockage fraction at 0.8° elevation (typically the lowest PPI tilt used in NAME) is shown in Fig. 1b. The simulation predicted many regions of over 90% blockage, as well as multiple blocks along single rays. Based on intercomparisons with real data, the simulations often did an excellent job of locating the positions of blocks. This was because there were no significant nonterrain blocks during NAME (e.g., trees, buildings, etc.) that would cause DEM-based correction to fail.

Once the simulated blockage pattern was calculated, each azimuth and range gate in real S-Pol data were matched to a corresponding simulated azimuth and range gate, and the estimated cumulative beam blockage fraction was used to increase the measured  $Z$  value similar to the "visibility correction" method of Germann et al. (2006). Corrections were applied as long as the beam blockage fraction did not exceed 90%, and there were no limitations on the maximum correction applied. This was more aggressive than the methodology of many

operational networks (e.g., Germann et al. 2006), in order to increase the amount of corrected data to compare with the polarimetric methods described below. Attempts to correct regions with greater than 90% blockage often led to the appearance of unrealistic reflectivity artifacts in the dataset, so these severely blocked regions were set to missing data.

### c. $K_{DP}$ method

A polarimetric correction methodology (hereafter referred to as the  $K_{DP}$  method) for horizontal reflectivity ( $Z_H$ ) was originally developed in 1999 following the TRMM Large-Scale Biosphere–Atmosphere Experiment (TRMM-LBA; Carey et al. 2000; Cifelli et al. 2002). The  $K_{DP}$  method, as described here, was used in the datasets analyzed by Nesbitt et al. (2008) and Rowe et al. (2008), and was a more sophisticated version of the PBB correction applied in Lang et al. (2007). A supplement to this description can be found online ([http://data.eol.ucar.edu/datafile/nph-get/82.119/readme\\_NAME\\_regional\\_radar\\_composites\\_v2.1.pdf](http://data.eol.ucar.edu/datafile/nph-get/82.119/readme_NAME_regional_radar_composites_v2.1.pdf)).

The  $K_{DP}$  method depends upon the self-consistency of polarimetric variables in rainfall (Goddard et al. 1994; Scarchilli et al. 1996; Ryzhkov et al. 2005) and the insensitivity of  $K_{DP}$  to PBB (Ryzhkov and Zrnić 1996; Zrnić and Ryzhkov 1996; Vivekanandan et al. 1999; Friedrich et al. 2007). The azimuthal trend of  $Z_H$  that satisfied  $1.5^\circ \leq K_{DP} < 2.0^\circ \text{ km}^{-1}$ , approximately corresponding to a rain rate ( $R$ ) of  $70 < R < 90 \text{ mm h}^{-1}$  (e.g., Bringi and Chandrasekar 2001), was examined in rainfall using the entire quality-controlled NAME S-Pol dataset. Data were limited to rain only through the use of the Tessendorf et al. (2005) hydrometeor identification algorithm at each examined data point.

Independent of blocking and other data quality control issues, this  $K_{DP}$  interval should result in a fixed range of  $Z_H$  in rain (Balakrishnan and Zrnić 1990) and extremely stable average values for  $Z_H$ . Indeed, during NAME in all unblocked, ocean-viewing azimuths ( $150^\circ$ – $340^\circ$ ) of 20–120-km range (Fig. 2), the median rain  $Z_H$  in this  $K_{DP}$  interval was 48.7 dBZ with a standard deviation of 4.2 dB. Moreover, median values of various smaller sample populations of unblocked  $Z_H$  in this  $K_{DP}$  interval were stable spatially (i.e., from ray to ray), and stable throughout the duration of the NAME project, with standard deviations  $\sim 0.3$  dB. One reason for this (besides the high-quality nature of the S-Pol data) is that this  $K_{DP}$  interval composed less than 1% of all nonzero  $K_{DP}$  values measured during NAME, thereby limiting the impact of DSD population variability on the  $K_{DP}$  PBB correction method.

Given this stability in high-quality rainfall measurements, any observed azimuthal variability in the median

$Z_H$  in this  $K_{DP}$  interval should be due to the effects of PBB. The reduction in median  $Z_H$  at a particular ray, relative to unblocked rays, is the decibel correction that must be added to all  $Z_H$  values in the blocked ray. For example, if the median unblocked  $Z_H$  is 48.7 dBZ, and a blocked azimuth has a median of 43 dBZ, then 5.7 dB must be added to all reflectivity data at that azimuth to correct for PBB effects.

Unfortunately, the blockage pattern in NAME was extremely complex, so the correction process was not as simple as this. Due to the existence of multiple blocks along certain rays in NAME, the azimuthal trend of  $Z_H$  was examined for two separate range groups—“inner” and “outer”—whose position varied by azimuth (Fig. 2). The position of a potential block was determined to within  $1^\circ$  azimuth and 1-km range by visual examination of maps of mean horizontal power (DM) in clear air, in the following way. No data within 20 km were examined because of the lack of PBB within this range. Beyond 20 km, each block was identified by the appearance of clutter in a specific ray followed by a rapid decline in DM. If two blocks occurred along a ray, the locations of the first and second blocks were noted. The range between the first and second blocks was assigned to the inner range group, and the range from the second block was assigned to the outer range group. No data beyond 120 km were examined, in order to minimize spatial resolution issues and because all blocks were within this range. No more than two blocks were identified in any ray using this methodology. If there was only one block, this was assigned to the outer range group.

For each blockage region (inner and outer), S-Pol rays were partitioned into  $0.8^\circ$  bins, which matched the azimuthal spacing of S-Pol during NAME. Median values of  $Z_H$  for each bin in the interval  $1.5^\circ \leq K_{DP} < 2.0^\circ \text{ km}^{-1}$  then were computed. Figure 3 shows the results of this analysis for all relevant  $0.8^\circ$  elevation data during NAME. While the outer range group was analyzed for all azimuths (Fig. 3a), the inner range group was needed only for a narrower sector where multiple possible blocks along single rays were identified (Fig. 2). In Fig. 3a, the median  $Z_H$  values from  $150^\circ$  to  $340^\circ$  azimuth were largely constant, indicating the lack of PBB (this sector was viewing the Gulf of California), while outside this region there was significant variability and often there were large reductions in median  $Z_H$ , sometimes of 20–30 dB. All azimuthal medians in the  $150^\circ$ – $340^\circ$  outer range  $Z_H$  data were averaged, and the result designated as  $Z_{\text{unblocked}}$ . The  $Z_H$  correction applied at a particular azimuth in a particular range group (inner or outer) was the difference between  $Z_{\text{unblocked}}$  and the median  $Z_H$  at that azimuth (diamonds in Fig. 3). The adjustment was not determined

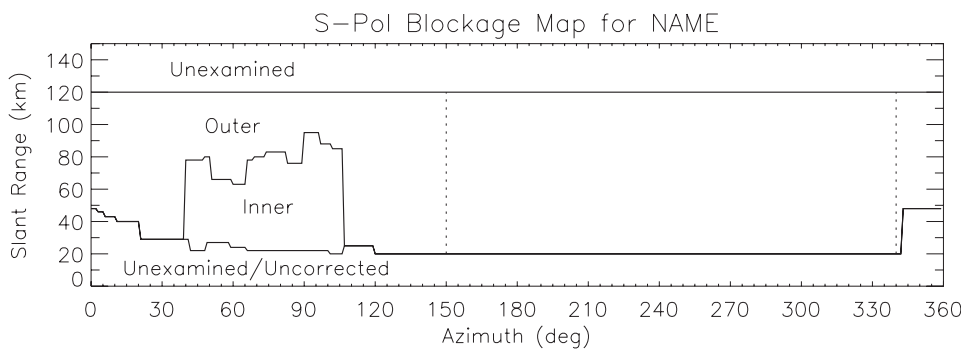


FIG. 2. Map of different blocked regions in the S-Pol's domain during NAME, showing inner and outer blockage regions, as well as uncorrected and unexamined regions. These regions were identified by visual analysis of clear-air power returns, and were used in the  $K_{DP}$ -based and fully self-consistent correction methodologies. The vertical dashed lines denote the ocean-viewing sector used in the development of both corrections.

on a volume-by-volume basis, but by estimating a mean adjustment over a large sample (the entire  $\sim 6$  week deployment period) at each azimuth.

The standard deviation of the unblocked azimuthal median  $Z_H$  values was 0.3 dB, which provided an empirical measure of the uncertainty in this correction, based on ray-to-ray variability in DSD populations, drop shapes, and statistical uncertainty. Additional un-

certainty would be introduced when applying the correction at each blocked azimuth, as there would be statistical uncertainty in the representativeness of the median  $Z_H$  value at that azimuth. Assuming normal populations, this additional uncertainty can be represented by the 95% confidence interval for each median. There were typically 400–500 points per azimuth available to estimate each median  $Z_H$ , which led to typical

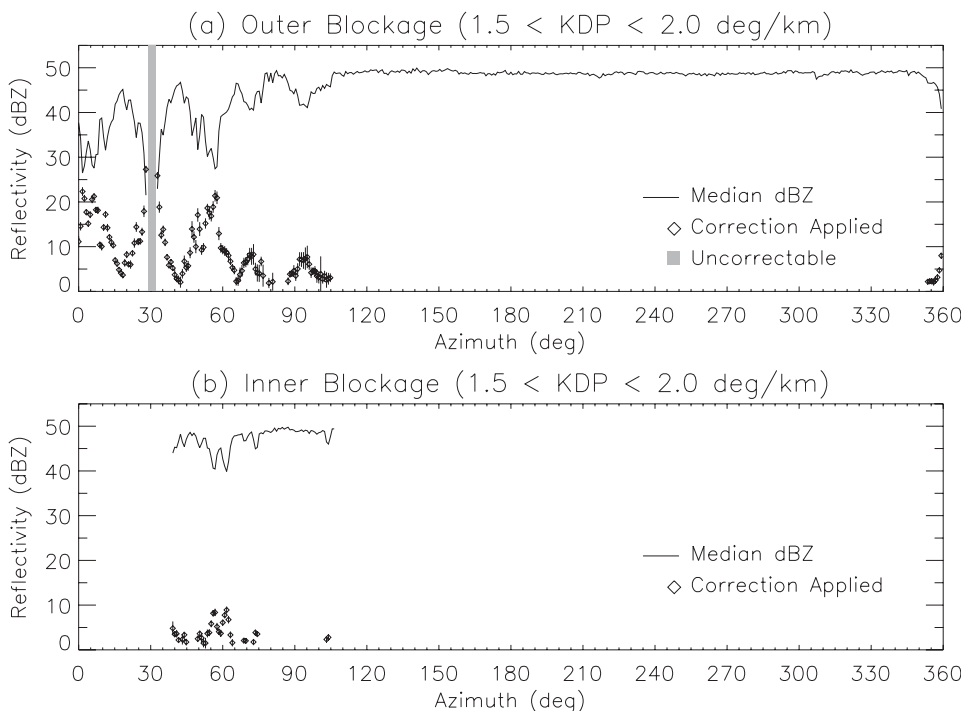


FIG. 3. Median reflectivity as a function of azimuth for rainfall  $K_{DP}$  values between  $1.5^\circ$  and  $2^\circ \text{ km}^{-1}$  over the entire S-Pol NAME dataset (line), reflectivity correction and estimated correction uncertainty applied at each blocked azimuth (diamonds with vertical lines), and uncorrectable azimuths (gray bar) for the (a) outer and (b) inner blocked ranges.

confidence intervals of  $\pm 0.5$  dB or better. However, some confidence intervals were much worse ( $> \pm 1$  dB), due to a lack of points. These were generally found in the outer blockage region in the azimuth range  $70^\circ$ – $100^\circ$ , where the slant range interval was fairly short (Fig. 2). Thus, the estimated uncertainties in the corrections at these azimuths were much higher than others (Fig. 3a).

The existence of some highly uncertain corrections at some azimuths was the reason for the limited division of the data (Fig. 2). In theory, however, given enough measurements (e.g., multiple seasons of observations), the radar data could be binned into extremely high-resolution spatial units (e.g.,  $1^\circ$  azimuth  $\times$  1 km range), and the corrections determined separately for each unit. The limiting factor is the number of appropriate  $K_{DP}$  measurements in that spatial unit. The  $K_{DP}$  method is highly dependent on a large sample size in order to reduce correction uncertainty. The number of points per spatial unit needed for  $\pm 1.5$  dB uncertainty in the correction is about 150–175, and about 350–375 points for  $\pm 1.0$  dB uncertainty, assuming similar behavior to the NAME observations. These uncertainty estimates do not take into account radar calibration uncertainties or departures in ray propagation paths from climatology.

Near  $30^\circ$  azimuth, there were several rays that were completely blocked at outer ranges (Fig. 3a), and no correction was possible because even the phase data were lost. These  $Z_H$  data were set to missing in all  $0.8^\circ$  elevation sweeps. This complete block did not exist at higher-elevation angles (e.g.,  $1.3^\circ$  and  $1.8^\circ$ , which were other common PPI tilts during NAME), and thus data near  $30^\circ$  azimuth were correctable in tilts higher than  $0.8^\circ$  elevation.

#### d. Fully self-consistent method

The fully self-consistent method (hereafter referred to as FSC method) was adapted from the studies of Giangrande and Ryzhkov (2005) and Ryzhkov et al. (2005). The FSC method also depends upon the self-consistency of polarimetric variables in rainfall (Goddard et al. 1994; Scarchilli et al. 1996; Ryzhkov et al. 2005), and the insensitivity of  $K_{DP}$  to PBB (Ryzhkov and Zrnić 1996; Zrnić and Ryzhkov 1996; Vivekanandan et al. 1999; Friedrich et al. 2007).

The FSC method first corrects the differential reflectivity ( $Z_{DR}$ ) for partial beam blockage effects in a way that is analogous to the  $K_{DP}$  method. Following the recommendations of Giangrande and Ryzhkov (2005) to examine  $Z_{DR}$  behavior in light rain or snowfall, the azimuthal trend of  $Z_{DR}$  in the “drizzle” hydrometeor category (Tessendorf et al. 2005) and where  $K_{DP} < 0.1 \text{ km}^{-1}$  was examined in the inner and outer blockage regions

defined in Fig. 2, for the entire NAME dataset (Fig. 4). Azimuths were binned by  $0.8^\circ$ , matching S-Pol’s azimuthal spacing during NAME. Based on the offset in the median  $Z_{DR}$  at a particular blocked azimuth, and the mean of the median  $Z_{DR}$  values in unblocked, ocean-viewing azimuths ( $150^\circ$ – $340^\circ$ ), a correction was applied to all  $Z_{DR}$  values at the blocked azimuth. Unlike what was done here, Giangrande and Ryzhkov (2005) recommended comparing  $Z_{DR}$  data from higher tilts to lower tilts at a particular azimuth to derive  $Z_{DR}$  offsets. This was not possible in the NAME dataset as higher tilts also suffered from significant PBB; so instead, unblocked ocean-viewing azimuths were used as the reference for correcting  $Z_{DR}$ .

The standard deviation of the collection of median values from the unblocked azimuths was 0.04 dB (less than 15% variability), suggesting very stable behavior in the light-rain median  $Z_{DR}$  values. Adding this uncertainty to the 95% confidence interval for the median  $Z_{DR}$  at each blocked azimuth resulted in uncertainty estimates for each corrected azimuth, which varied somewhat but averaged  $\sim 0.1$  dB due to the large number of samples available for light rain (mean number of points per azimuth was greater than 13 000; see Fig. 4). As with the  $K_{DP}$  method, this uncertainty does not take into account radar calibration uncertainties or departures in ray propagation paths from climatology.

There is some debate in the literature over whether  $Z_{DR}$  truly is affected by PBB, with Carey et al. (2000) and Giangrande and Ryzhkov (2005) demonstrating evidence for, and Friedrich et al. (2007) demonstrating evidence against. Based on Fig. 4,  $Z_{DR}$  clearly was affected by PBB in the NAME dataset, and the magnitude of the effect (which could lead to reductions in excess of 1 dB) increased roughly with the strength of the block (cf. Figs. 3 and 4). Indeed, for azimuths with nonzero  $Z_H$  corrections (Fig. 3), the  $K_{DP}$  method’s  $Z_H$  corrections were positively correlated with estimated  $Z_{DR}$  corrections, with a correlation coefficient of 0.89. However,  $Z_{DR}$  often was stable in weaker PBB ( $< 10$  dB  $Z_H$  reduction), particularly in the inner blockage region where no correction was necessary (Fig. 4b). While there was no clear threshold, corrections to  $Z_{DR}$  became necessary when  $K_{DP}$  method-estimated  $Z_H$  reductions were on the order of 2–9 dB, depending on azimuth.

Once  $Z_{DR}$  was corrected for PBB, a NAME self-consistency relationship for  $Z_H$ ,  $Z_{DR}$ , and  $K_{DP}$  was developed using all available rain-identified (Tessendorf et al. 2005) data from unblocked, ocean-viewing azimuths ( $150^\circ$ – $340^\circ$ ) and ranges between 20 and 90 km, following the methodology of Ryzhkov et al. (2005). The derived consistency relationship was

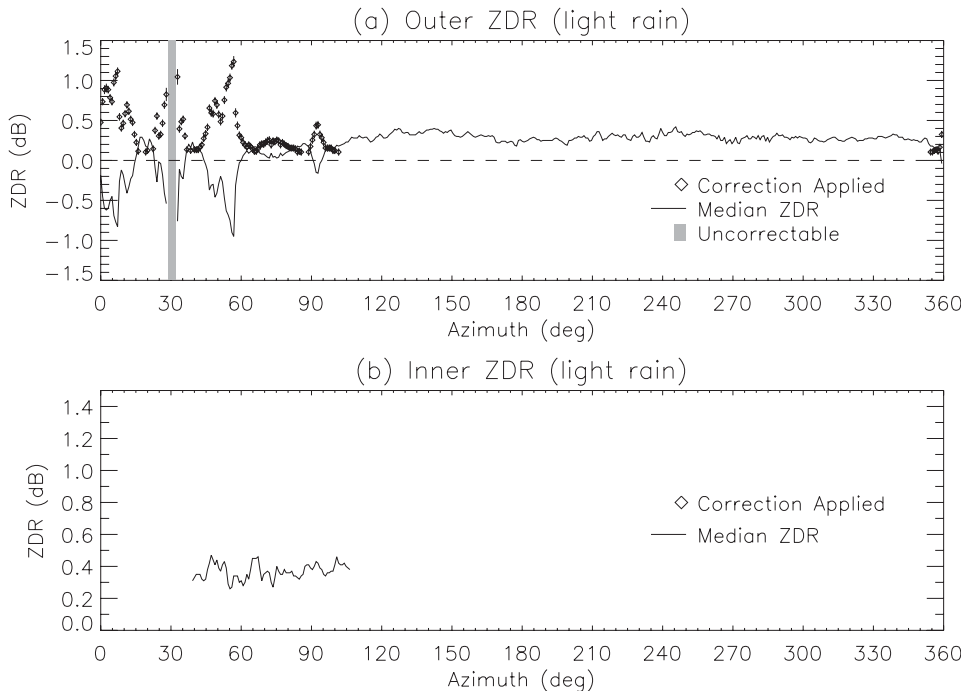


FIG. 4. Median differential reflectivity ( $Z_{DR}$ ) as a function of azimuth for light drizzle where  $K_{DP} < 0.1^\circ \text{ km}^{-1}$  over the entire S-Pol NAME dataset (line),  $Z_{DR}$  correction and estimated correction uncertainty applied at each blocked azimuth (diamonds with vertical lines), and uncorrectable azimuths (gray bar) for (a) the outer blocked ranges. The horizontal dashed line is simply  $Z_{DR} = 0$  dB. (b) Shown are the inner blocked ranges. No corrections were applied at inner ranges due to the lack of significant reductions in  $Z_{DR}$ .

$$Z_H = 41.4 + 11.2 \log_{10}(K_{DP}) + 4.2Z_{DR}. \quad (1)$$

Using this relationship, the integrals

$$I_1 = \int_{Z_{MIN}}^{Z_{MAX}} \langle K_{DP}(Z) \rangle n(Z) dZ \quad (2)$$

and

$$I_2 = \int_{Z_{MIN}}^{Z_{MAX}} 10^{-41.4/11.2 + Z/11.2 - c(Z_{DR}(Z))/11.2} n(Z) dZ \quad (3)$$

were matched in rain-identified (Tessendorf et al. 2005) data in blocked regions by increasing  $Z_H$ , following Ryzhkov et al. (2005) and Giangrande and Ryzhkov (2005). Here,  $\langle f(Z) \rangle$  refers to the average value of variable  $f$  as a function of  $Z$ , and  $n(Z)$  refers to the number of points at that value of  $Z$  (1-dB intervals were used to bin up the  $Z$  data). The Ryzhkov studies provided a large amount of flexibility in choosing the area-time domain for computing these integrals, with the only stipulation being that  $I_1 > 200^\circ \text{ km}^{-1}$  (i.e., there be enough rain) to keep errors low.

For this study the time domain was the entire project, and the area domains were set up almost exactly like they were for the  $K_{DP}$  method and the  $Z_{DR}$  correction (Fig. 2), with azimuths in the inner and outer regions

binned into  $1^\circ$  units (because the full spectrum of rain was considered for the entire dataset, computer memory usage was excessive if  $0.8^\circ$  azimuthal bins were used). In this case,  $I_1$  averaged about  $6800^\circ \text{ km}^{-1}$  per azimuth, with a standard deviation of  $3300^\circ \text{ km}^{-1}$ . While this greatly exceeded the requirements for  $I_1$ , it did not exceed it to the point that the data could have been grouped into extremely high resolution bins (e.g., 1 km range  $\times$   $1^\circ$  azimuth units). Therefore, temporal and spatial domains were kept similar to before, to aid with intercomparisons between the different methods.

Figure 5 shows the resulting corrections for the FSC method compared to those derived from the  $K_{DP}$  method. While the general patterns were similar, there were some noted areas of disagreement, which will be examined in more detail in the next section. Typically, however, if there was disagreement, the  $K_{DP}$  method tended to produce a higher correction than the FSC method.

### 3. Results

#### a. Correction example

The three correction techniques were applied to six different volumes from NAME. These volumes were chosen to match the notable TRMM overpasses during NAME as discussed later. Figure 6 shows an example of

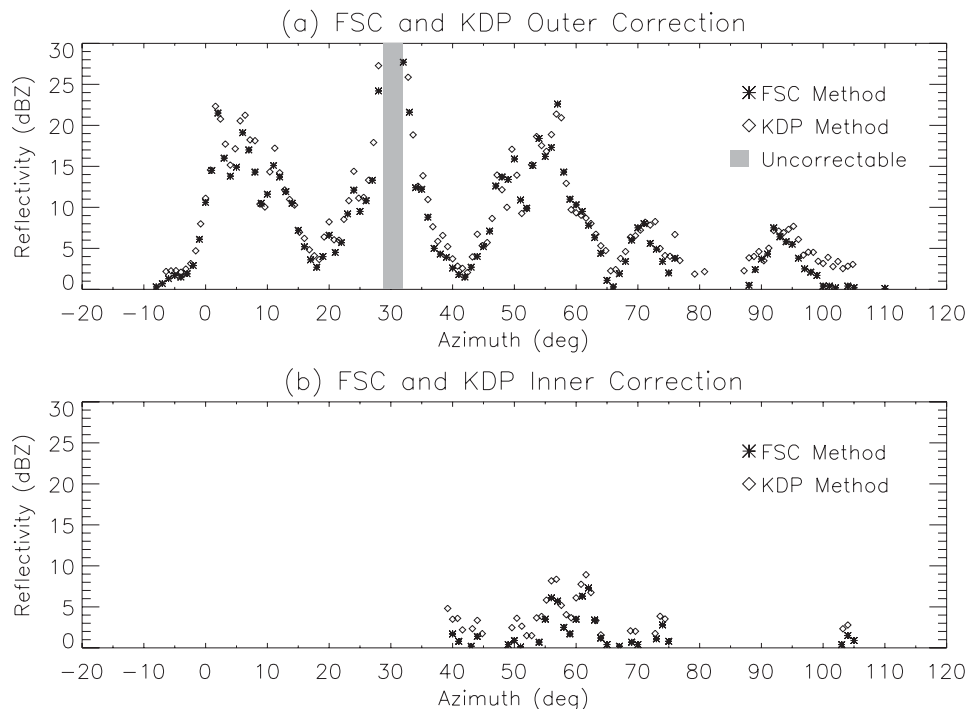


FIG. 5. Corrections applied at blocked azimuths using the  $K_{DP}$  method (diamonds; same as in Fig. 3) and the fully self-consistent method (FSC; asterisks). The gray bar denotes azimuths uncorrectable by either method.

the relative performance of the three corrections, as functions of azimuth. When considering the full rays (including inner and outer blockage ranges when applicable; see Fig. 6a), it was difficult to evaluate the DEM method against the other two. This was because the DEM method was not applied where the estimated blockage exceeded 90%. This led to 56° of azimuth at 0.8° elevation being uncorrectable at varying ranges, as opposed to only 3° being uncorrectable by the  $K_{DP}$  and FSC methodologies (Fig. 5a). Even relaxing this constraint would not have helped much, as 41° of azimuth were affected by an estimated 100% blockage in the DEM model. Therefore, in Fig. 6a only DEM rays with at least 50% of the points available to the other two techniques were considered, but the entire ray lengths are compared. In Fig. 6b, only corrections along the ray lengths available to the DEM method are compared (i.e., regions not colored black in Fig. 1b).

Between 350° (−10° in Fig. 6) and 50° azimuth, there was fairly good agreement between the different methodologies where they could be compared, with offsets typically in the range of 1–2 dB. Some exceptions occurred in sharp gradients in PBB patterns, like near 0° and on either side of 30°. From 50° to 110° azimuth, the agreement was much worse, however. The DEM and  $K_{DP}$  methods applied corrections at many azimuths

where FSC did nothing, and the DEM method was much more aggressive than the other two. It is unclear whether this was the result of an imperfect DEM model (entirely plausible considering the overprediction of 100% blockage), or weaknesses in our method for estimating block locations in the  $K_{DP}$  and FSC schemes (section 2c), or both.

The radar clutter pattern appeared to be more complex in this azimuthal band, with some clutter observable out to 120-km range (not shown), although south of 60° azimuth, there was much less PBB than for more northerly azimuths. Subsectioning the radar data into smaller spatial bins may have helped to improve the agreement between the polarimetric and DEM methodologies in this region, and the differences between the polarimetric methodologies themselves may be due to noisy corrections in this azimuthal band, particularly for the  $K_{DP}$  method (Fig. 3a). This is an excellent example of where having more data would be helpful, as it would allow the radar observations to be subsectioned into smaller spatial bins while still preserving low uncertainties in the corrections.

Overall, the FSC method tended to not correct as much as the  $K_{DP}$  method. The DEM method often over- or undercorrected relative to the polarimetric methods depending on azimuth.

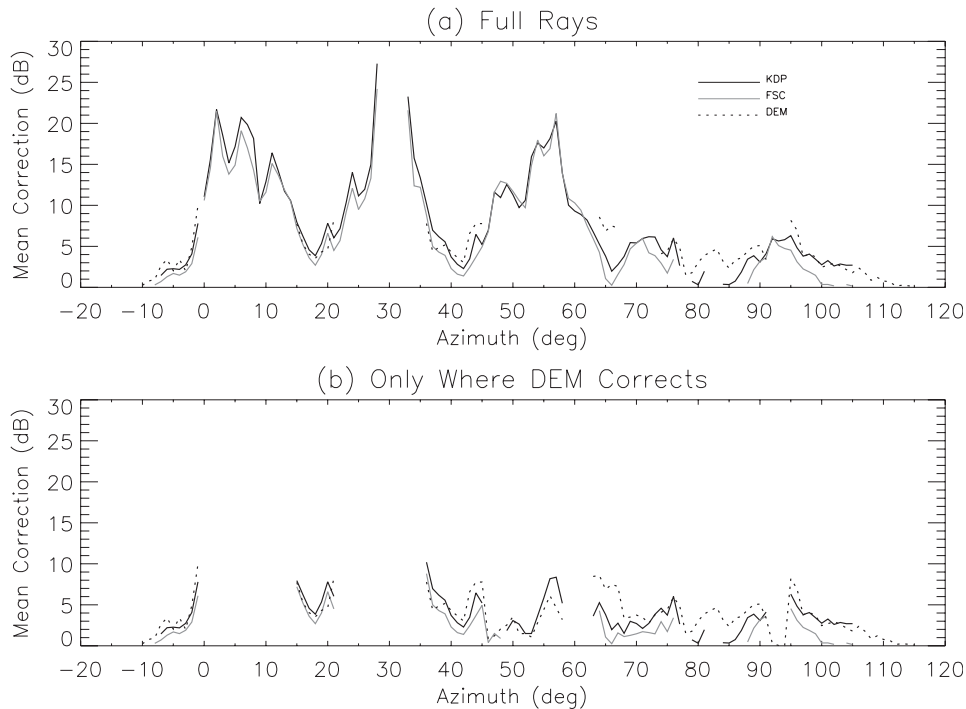


FIG. 6. Mean corrections by azimuth applied to the  $0.8^\circ$  S-Pol sweeps from the following dates and times: 2128 UTC 12 Jul, 0157 UTC 7 Aug, 0045 UTC 10 Aug, 2238 UTC 13 Aug, 2032 UTC 17 Aug, and 0304 UTC 18 Aug 2004. Data were corrected using the  $K_{DP}$  method (KDP; solid black line), the DEM method (DEM; dotted black line), and the fully self-consistent method (FSC; solid gray line). Corrections of 0 dB are not plotted. (a) Full rays considered, but DEM-corrected rays with less than 50% of the points in the other corrected rays are not shown (i.e., rays that were blocked over 90% along much of their length). (b) Only the portions of the rays available for correction using DEM are shown (i.e., less than 90% estimated blockage).

### b. TRMM intercomparisons

Intercomparisons of corrected NAME S-Pol  $Z_H$  results with six TRMM PR overpasses during NAME were performed. These were the only overpasses with significant precipitation in S-Pol's blocked regions that occurred during NAME, as TRMM's overflight schedule often coincided with the minimum in the NAME precipitation diurnal cycle (Lang et al. 2007). The PR is a well-calibrated radar system that has been successfully used to calibrate reflectivity from ground radars to within 1–1.5 dB (Anagnostou et al. 2001), and was the only realistic means of cross-checking the S-Pol correction methodologies in NAME. That being said, the PR's operating frequency of 14 GHz (Ku band) is affected by attenuation in heavy rain. The 2A25 (version 6) algorithm uses a blended surface reference technique and a Hitschfeld–Bordan (Hitschfeld and Bordan 1954) technique to estimate path-integrated attenuation, which is then used to correct the reflectivity profile as a function of range (Iguchi et al. 2000).

S-Pol data were interpolated to the same horizontal grid as the PR data as follows. The quality-controlled

S-Pol sweep closest in time (always within 2 min) to each TRMM overpass was selected. As with the DEM correction, standard atmosphere propagation of the S-Pol's beam was assumed. To match reflectivity between the two radars at each PR grid point, S-Pol gates were selected if they were within 5 km horizontally and 250 m vertically of each PR gridpoint location. Furthermore, it was required that at least eight ground radar points had valid meteorological echoes. These valid S-Pol reflectivity points were then averaged in linear reflectivity space (i.e.,  $\text{mm}^6 \text{m}^{-3}$ ) for comparison with TRMM.

Figure 7 shows the resultant reflectivity difference distributions for all overpasses, and Table 1 shows the statistical results from the intercomparisons, including individual overpasses. There were six points of comparison: high-altitude S-Pol data unaffected by blockage and above the melting level (PR-SPOL); low-altitude S-Pol data in the western half of the S-Pol's domain, which was largely free of terrain blockage (PR-UNBL; see Fig. 1b); low-altitude data in S-Pol's northeastern quadrant (which was subject to terrain blockage; Fig. 1b), below the melting level to avoid brightband contamination, and corrected via the  $K_{DP}$  method (PR-KDP); the same

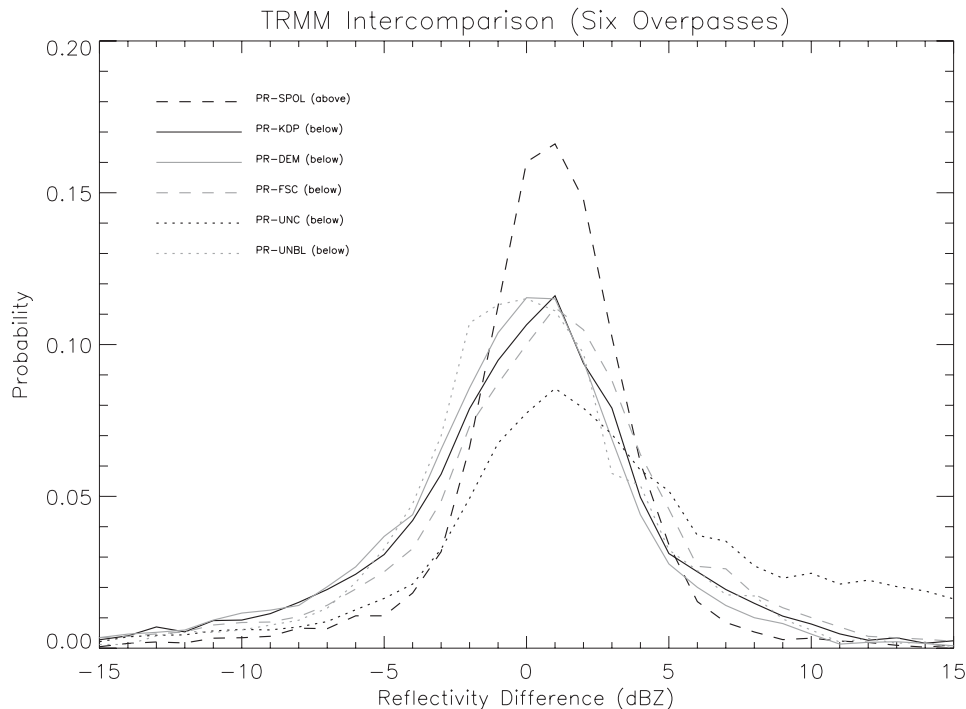


FIG. 7. Intercomparisons between TRMM and S-Pol reflectivities for six overpasses during NAME 2004, with TRMM PR minus S-Pol where height  $\geq 6$  km MSL and elevation  $>1.8^\circ$  (PR-SPOL; dashed black line), PR minus  $K_{DP}$ -corrected data in the S-Pol's NE quadrant where height  $\leq 4$  km MSL and elevation  $\leq 1.8^\circ$  (i.e., blocked; PR-KDP; solid black line), PR minus DEM-corrected data in blocked regions (PR-DEM; solid gray line), PR minus fully self-consistent-corrected data in blocked regions (PR-FSC; dashed gray line), PR minus uncorrected S-Pol data in blocked regions (PR-UNC; dotted black line), and PR minus uncorrected and unblocked S-Pol data in S-Pol's western domain where height  $\leq 4$  km MSL and elevation  $\leq 1.8^\circ$  (PR-UNBL; dotted gray line). Note that only points with TRMM reflectivities  $>18$  dBZ were considered.

low-altitude data corrected via the DEM method (PR-DEM); the same low-altitude data corrected via the FSC method (PR-FSC); and the same but uncorrected low-altitude data (PR-UNC).

In the high-altitude data, there was a high variance in the distribution of PR-SPOL  $Z_H$  values, which was expected given the radically different radar configurations, as well as different beam and scan geometries (Fig. 7; see also Anagnostou et al. 2001). The mean offset between radar systems varied depending on overpass, but the mean value over all overpasses was +1.1 dB (Table 1), within the uncertainty range of Anagnostou et al. (2001), and suggesting that S-Pol was well calibrated relative to TRMM outside of blocked areas.

Comparing low-altitude data between these two radars was more problematic, because of the uncertainty in correcting TRMM's reflectivity profiles for attenuation (Iguchi et al. 2000) in heavy convective rain, or in situations with a radar bright band (stratiform). Both of these situations would cause the uncertainty in attenuation correction to be highest near the surface since the

path-integrated attenuation is maximized at the farthest range. Thus, comparisons of S-Pol with TRMM reflectivities at low altitude should be considered with more caution than the high-altitude comparisons. Analysis of 2502 PR-UNBL points from all six overpasses resulted in a mean offset of +0.5 dB (Table 1), which suggests that the TRMM attenuation correction scheme was working well for these NAME cases, and that meaningful low-altitude intercomparisons between TRMM and S-Pol could be made.

Despite having a mode near +1 dB, the PR-UNC distribution (Fig. 7) contained a high relative frequency of points at large positive offsets, showing the effects of severe beam blockage on these uncorrected data. This led to a large mean overall offset (+4.2 dB) as well as large offsets during individual overpasses (Table 1). These large positive offsets were removed by all of the correction methodologies (Fig. 7), achieving mean overall offsets below the uncertainty level expected in TRMM intercomparisons (1–1.5 dB; Table 1). Although individual overpasses should not be emphasized given

TABLE 1. Mean offsets between TRMM and S-Pol reflectivities plus total number of points analyzed for six overpasses during NAME 2004, with TRMM PR minus S-Pol where height  $\geq 6$  km MSL and elevation  $>1.8^\circ$  (i.e., unblocked; PR-SPOL), PR minus S-Pol in unblocked low-altitude regions in S-Pol's western domain where height  $\leq 4$  km MSL and elevation  $\leq 1.8^\circ$  (PR-UNBL),  $K_{DP}$ -corrected data (PR-KDP) in blocked regions (NE S-Pol quadrant where height  $\leq 4$  km MSL and elevation  $\leq 1.8^\circ$ ), PR minus DEM-corrected data in blocked regions (PR-DEM), PR minus FSC-corrected data (PR-FSC), and PR minus uncorrected S-Pol data in blocked regions (PR-UNC). Also listed are overall amounts considering all six overpasses. Only points with TRMM reflectivities  $>18$  dBZ were considered. Means not computed for intercomparisons with fewer than 100 points.

|                       | 2128 UTC<br>12 Jul | 0157 UTC<br>7 Aug | 0045 UTC<br>10 Aug | 2238 UTC<br>13 Aug | 2032 UTC<br>17 Aug | 0304 UTC<br>18 Aug | Overall |
|-----------------------|--------------------|-------------------|--------------------|--------------------|--------------------|--------------------|---------|
| PR-SPOL mean (dB)     | +0.000             | +1.536            | +1.696             | +1.269             | -0.508             | +1.166             | +1.113  |
| PR-SPOL No. of points | 535                | 330               | 1891               | 304                | 521                | 2807               | 6388    |
| PR-UNBL mean (dB)     | NA                 | NA                | +0.141             | NA                 | NA                 | +1.195             | +0.464  |
| PR-UNBL No. of points | 0                  | 9                 | 1186               | 38                 | 71                 | 1198               | 2502    |
| PR-KDP mean (dB)      | -0.717             | +0.286            | +0.048             | -1.111             | -1.102             | +1.352             | +0.272  |
| PR-KDP No. of points  | 647                | 1107              | 558                | 361                | 1025               | 2462               | 6160    |
| PR-DEM mean (dB)      | -0.957             | -0.875            | +0.240             | -1.131             | -2.609             | +1.118             | -0.226  |
| PR-DEM No. of points  | 555                | 879               | 321                | 325                | 821                | 2288               | 5189    |
| PR-FSC mean (dB)      | +0.076             | +1.279            | +1.116             | -0.957             | -0.565             | +1.925             | +0.958  |
| PR-FSC No. of points  | 647                | 1107              | 558                | 361                | 1025               | 2462               | 6160    |
| PR-UNC mean (dB)      | +2.921             | +5.145            | +9.057             | +0.891             | +3.275             | +3.803             | +4.169  |
| PR-UNC No. of points  | 647                | 1107              | 558                | 361                | 1025               | 2462               | 6160    |

that many of them have relatively few points for intercomparison, this level of accuracy also was achieved for most or all overpasses depending on the methodology. As seen in Fig. 6, the FSC method did not apply as much correction as the other two methods, leading to a larger positive offset with TRMM (although still within the expected accuracy of the intercomparison). Overall, these results show that each of the examined PBB-correction methods improved upon the TRMM intercomparisons with uncorrected data, achieving excellent agreement with TRMM in the volumetric sense.

Based on Fig. 6, according to all correction schemes, the  $0^\circ$ - $60^\circ$  azimuth band was affected by much more severe blockage than that at  $60^\circ$ - $90^\circ$ . For example, the average correction per ray for the  $K_{DP}$  method was +11.5 dB in the  $0^\circ$ - $60^\circ$  band, but only +3.7 dB within  $60^\circ$ - $90^\circ$ . To assess the correction performance in high ( $<-10$  dB) and low ( $>-10$  dB) occultation regions, Table 2 examines the relative performance of the different correction schemes against TRMM for these two azimuth groups. Similar trends were seen to the previous ones, with all methods correcting to within the uncertainty of the TRMM intercomparison. However, the DEM method suffered in the high-occultation azimuths as nearly 25% fewer points were available for correction compared to other methods; in essence, due to the 90% blockage criterion, both azimuth regions counted as low occultation for the DEM method. Both  $K_{DP}$  and FSC performed well in the high-occultation region. In the low-occultation region, which also was marked by a complex clutter map (section 3a), all methods compared favorably to TRMM despite the sometimes large ray-to-

ray disagreements between them, as seen in Fig. 6. This may have been a consequence of the spatial averaging that was required by the TRMM intercomparisons. That is, while high-resolution polar-coordinate data showed some disagreements between the methodologies, these differences were much reduced in the lower-resolution gridded data.

### c. Seasonal mean

A major limitation to the examined PBB-correction methodologies was that unrecoverably blocked echoes could not be corrected (e.g., Fig. 3a). Weaker echoes were lost, particularly at longer ranges where the minimum detectable reflectivity was larger for a given noise threshold. The loss of these weaker echoes should lead to biases in severely blocked rays in  $Z_H$  or rain climatologies, particularly at long ranges.

Figure 8 shows the mean  $Z_H$  for the entire NAME deployment. This was a composite ray-based (i.e., not Cartesian gridded) product using  $0.8^\circ$  elevation PPI data corrected via the  $K_{DP}$  method. There were distinct azimuthal-dependent low biases at long ranges. Based on comparison with Fig. 3, the lowest mean reflectivities tended to be situated behind the worst blocks. Indeed, there were several rays near  $30^\circ$  that lacked corrected data altogether; this shows up as the large data gap in Fig. 8. These, and other severely blocked rays, may benefit from VPR correction or the use of well-placed rain gauges. However, for NAME, no such rain gauges were available, and a better understanding of the vertical structure of precipitating systems and its variability

TABLE 2. Similar to Table 1 but only showing the overall reflectivity offsets and points, and with S-Pol's NE quadrant broken down into relatively high-occultation ( $0^{\circ}$ – $60^{\circ}$  azimuth) and relatively low-occultation regions ( $60^{\circ}$ – $90^{\circ}$  azimuth). PR-SPOL and PR-UNBL not considered.

|                                    | Overall offset (dB) | Total No. of points |
|------------------------------------|---------------------|---------------------|
| PR-KDP $0^{\circ}$ – $60^{\circ}$  | –0.011              | 4000                |
| PR-DEM $0^{\circ}$ – $60^{\circ}$  | –0.280              | 3105                |
| PR-FSC $0^{\circ}$ – $60^{\circ}$  | +0.701              | 4000                |
| PR-UNC $0^{\circ}$ – $60^{\circ}$  | +5.299              | 4000                |
| PR-KDP $60^{\circ}$ – $90^{\circ}$ | +0.797              | 2160                |
| PR-DEM $60^{\circ}$ – $90^{\circ}$ | –0.147              | 2084                |
| PR-FSC $60^{\circ}$ – $90^{\circ}$ | +1.435              | 2160                |
| PR-UNC $60^{\circ}$ – $90^{\circ}$ | +2.076              | 2160                |

as a function of terrain would be needed to employ VPR correction properly (section 1b).

#### 4. Conclusions

Three methodologies for correcting  $Z_H$  in the presence of PBB have been outlined and tested using severely blocked radar data from a major field campaign in the tropics. One methodology was based on simulated radar beam interactions with terrain using a DEM.

Two methodologies invoke the self-consistency of polarimetric variables in rainfall, and the relative insensitivity of  $K_{DP}$  to PBB. Intercomparisons between corrected ground radar data and selected TRMM satellite overpasses suggest that all of the methodologies could correct mean  $Z_H$  to within the expected uncertainty of such intercomparisons (1–1.5 dB). All methods proved to be advantageous over not correcting the data at all, within the limitations imposed by comparisons with TRMM. This fundamental agreement with TRMM occurred regardless of whether regions of relatively more severe or regions of relatively less severe blockage were analyzed.

However, sometimes there was significant ray-to-ray variability in the behavior of the corrections, and they did not always agree to within 1–2 dB. The worst agreement occurred where azimuthal gradients were the strongest, and where terrain clutter patterns were the most complex. One potential reason for the discrepancies in gradient regions could be that, in this study, the  $K_{DP}$  method used  $0.8^{\circ}$  azimuthal bins for its corrections, while the other methods used  $1^{\circ}$  azimuthal resolution. Also, these gradient regions tended to have fewer data points available for developing the polarimetric corrections. Finally, sharp azimuthal gradients may cause additional

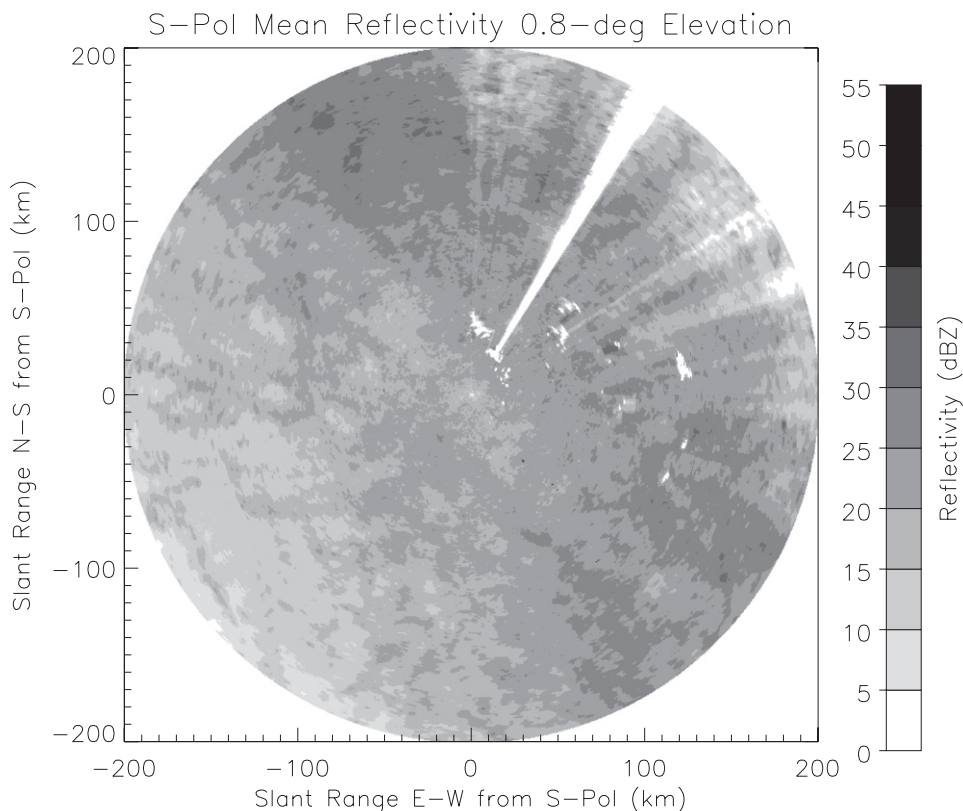


FIG. 8. Mean S-Pol reflectivity over the entire NAME 2004 deployment at  $0.8^{\circ}$  elevation.

quality-control issues related to radar beamwidth, antenna sidelobe patterns, etc. Improvements in the methodologies, either through more sophisticated terrain-beam interaction modeling or additional seasons of radar data, may help to alleviate these discrepancies. In addition, these disagreements were reduced in lower-resolution gridded data, which often have been the focus of analyses (e.g., Nesbitt et al. 2008; Rowe et al. 2008). Provided all of the above is true, then actual correction performance may not be the determining factor in choosing which correction methodology to apply to a dataset. Thus, the relative advantages and disadvantages of each methodology should be discussed.

The main advantage of the DEM method is that it does not require any radar data to “spin up” the correction. Thus, prior to a field campaign the correction factors for each affected radar gate could be developed and applied, even in real time. Whereas the polarimetric methods require substantial amounts of rainfall data from partially blocked regions, for each relevant range, azimuth, and elevation angle bin, the DEM method would be immune to those concerns, allowing it to be applied to extremely small datasets, winter field projects with mostly snowfall, scans above the freezing-level altitude, or uncommon or irregular scans (e.g., scattered, infrequent RHIs).

The DEM method greatly benefits from having a sophisticated terrain-beam interaction model, and high-resolution DEM data, in order to minimize the errors in estimated correction factors. The simple DEM methodology used in this study clearly was inadequate as it could not correct as much data as the polarimetric methodologies. Use of a higher-resolution DEM, an updated refractivity profile, or a more elaborate methodology (e.g., Pellarin et al. 2002) could improve such an approach. However, correction of 90%+ blockage using DEMs is a difficult challenge that is normally not attempted (e.g., Germann et al. 2006). Another major concern is blockage caused by nonterrain features, such as trees or buildings. This was not a concern in NAME, but often is in other deployments (e.g., Carey et al. 2000; Cifelli et al. 2002). A DEM methodology alone cannot deal with such blockages.

The two tested polarimetric correction methodologies share some advantages. Each will be applicable as long as the radar signal is above the noise, regardless of what causes the block (terrain, vegetation, buildings, etc.). Indeed, in NAME both methods corrected data in regions where the DEM-estimated blockage was 90%–100%, and agreement was excellent with TRMM even in the most highly occulted azimuth region ( $0^{\circ}$ – $60^{\circ}$ ). While having unblocked sectors of rainfall data helps with the development of the tuned self-consistency relationships

used by these correction methodologies, such relationships could be accurately derived from disdrometer data, or taken from the existing literature with some additional correction uncertainty (e.g., Balakrishnan and Zrnić 1990; Ryzhkov et al. 2005).

Compared to the fully self-consistent method (Giangrande and Ryzhkov 2005), the  $K_{DP}$  methodology can be used without correcting  $Z_{DR}$  first (or at all), and does not require the development and usage of a self-consistency relationship of the form  $Z_H = f(Z_{DR}, K_{DP})$ . It is thus somewhat simpler to implement and avoids errors caused by  $Z_{DR}$  miscalibration (at the expense of requiring  $Z_H$  to be calibrated). However, the  $K_{DP}$  method has by far the most data requirements. Correction factors will be highly uncertain in azimuths with little data in moderate to heavy rainfall. On the other hand, this method also benefits the most from additional data, as correction uncertainties may be driven down to potentially lower values than other correction methodologies in large datasets, assuming median  $Z_H$  values remain stable for the examined  $K_{DP}$  interval.

Apart from the other benefits discussed already, the fully self-consistent method is advantageous in that it can be used as an absolute calibration of  $Z_H$ , whereas the other two methods are relative calibrations and thus require  $Z_H$  to be well calibrated beforehand. Depending on the time period used in the area-time integrals of  $K_{DP}$  and  $Z_{DR}$ , the FSC method also could be less vulnerable to changes in ray propagation paths, which would change the magnitude of the observed PBBs over time. As applied in this study, however, the FSC method was just as vulnerable as the other two to this problem. In essence, shorter integration times can reduce the impact of ray propagation variability, but at the expense of introducing larger errors due to temporal DSD variability. Thus, there is additional flexibility in the FSC method compared to the  $K_{DP}$  method, which is forced to use as long an integration time as possible to keep errors low, but this flexibility does not exist without a trade-off.

Departures in ray propagation paths from climatology are less of a concern in the tropics, with its weaker spatial and temporal variabilities in the atmospheric state (apart from nocturnal inversions and topographic flows), but they are important in the midlatitudes. Also, in situations where blocks are caused by vegetation, power reduction values could change over the course of a season as the biota changes. Caution should be exercised when applying the correction methodologies in these situations, and appropriate measures should be taken to mitigate these issues when possible (e.g., updating the DEM model with the new atmospheric state, shortening the integration time used in the FSC method, etc.).

A major weakness of the examined PBB-correction techniques (DEM and polarimetric) was the inability to correct whenever the original signal was reduced to noise, which occurred whenever weak echoes passed behind blocks of sufficient strength. For example, if at a particular range a radar has a minimum detectable reflectivity of 0 dBZ, but there is a 10-dB block obstructing the view at that range, then echoes of 10 dBZ or less would not be detectable by the radar. This can result in missing echoes in individual sweeps, and in biases in the corrected reflectivity and rainfall climatologies. This will happen even if  $K_{DP}$  is used to estimate rainfall, as phase data are lost in these situations as well. What happens is that the typically more common weaker echoes are not observed, while the less-frequent stronger echoes are observed. This will lead to a low bias in unconditional mean echo, but a high bias in conditional mean echo values. These biases will be most important at long ranges, where minimum detectable reflectivities normally are reduced even under unblocked conditions. Severely blocked rays such as these may be good candidates for the use of VPR or rain gauge-based corrections, if such data are available.

*Acknowledgments.* The NAME project was supported by the National Oceanic and Atmospheric Administration and the National Science Foundation (NSF). S-Pol radar observations and the presented analyses for NAME were funded by NSF. The authors thank the following people for their assistance with this research: Dr. Steven A. Rutledge, Dr. Walt Petersen, Dr. Robert Cifelli, and Paul Hein.

#### REFERENCES

- Anagnostou, E. N., C. A. Morales, and T. Dinku, 2001: The use of TRMM Precipitation Radar observations in determining ground radar calibration biases. *J. Atmos. Oceanic Technol.*, **18**, 616–628.
- Andrieu, H., J. D. Creutin, G. Delrieu, and D. Faure, 1997: Use of a weather radar for the hydrology of a mountainous area. Part I: Radar measurement interpretation. *J. Hydrol.*, **193**, 1–25.
- Balakrishnan, N., and D. S. Zrnić, 1990: Estimates of rain and hail rates in mixed-phase precipitation. *J. Atmos. Sci.*, **47**, 565–583.
- Battán, L. J., 1973: *Radar Observation of the Atmosphere*. University of Chicago Press, 324 pp.
- Bech, J., B. Codina, J. Lorente, and D. Bebbington, 2003: The sensitivity of single polarization weather radar beam blockage correction to variability in the vertical refractivity gradient. *J. Atmos. Oceanic Technol.*, **20**, 845–855.
- Bringi, V. N., and V. Chandrasekar, 2001: *Polarimetric Doppler Weather Radar: Principles and Applications*. Cambridge University Press, 636 pp.
- Carey, L. D., R. Cifelli, W. A. Petersen, and S. A. Rutledge, 2000: Preliminary report on TRMM-LBA rainfall estimation using the S-Pol radar. Dept. of Atmospheric Science Paper 697, Colorado State University, Fort Collins, CO, 19 pp. [Available online at [http://radarmet.atmos.colostate.edu/trmm\\_lba/spol\\_rain\\_info/PrelimRptLBASPOLrain.pdf](http://radarmet.atmos.colostate.edu/trmm_lba/spol_rain_info/PrelimRptLBASPOLrain.pdf).]
- Cifelli, R., W. A. Petersen, L. D. Carey, S. A. Rutledge, and M. A. F. Silva Dias, 2002: Radar observations of kinematic, microphysical, and precipitation characteristics of two MCSs in TRMM LBA. *J. Geophys. Res.*, **107**, 8077, doi:10.1029/2000JD000264.
- Creutin, J. D., H. Andrieu, and D. Faure, 1997: Use of a weather radar for the hydrology of a mountainous area. Part II: Radar measurement validation. *J. Hydrol.*, **193**, 26–44.
- Dinku, T., E. N. Anagnostou, and M. Borge, 2002: Improving radar-based estimation of rainfall over complex terrain. *J. Appl. Meteor.*, **41**, 1163–1178.
- Friedrich, K., U. Germann, J. J. Gourley, and P. Tabary, 2007: Effects of radar beam shielding on rainfall estimation for the polarimetric C-band radar. *J. Atmos. Oceanic Technol.*, **24**, 1839–1859.
- Germann, U., and J. Joss, 2003: Operational measurement of precipitation in mountainous terrain. *Weather Radar: Principles and Advanced Applications*, P. Meischner, Ed., Springer-Verlag, 52–77.
- , G. Galli, M. Boscacci, and M. Bolliger, 2006: Radar precipitation measurement in a mountainous region. *Quart. J. Roy. Meteor. Soc.*, **132**, 1669–1692.
- Giangrande, S. E., and A. V. Ryzhkov, 2005: Calibration of dual-polarization radar in the presence of partial beam blockage. *J. Atmos. Oceanic Technol.*, **22**, 1156–1166.
- Gochis, D. J., C. J. Watts, J. Garatuza-Payan, and J. Cesar-Rodriguez, 2007: Spatial and temporal patterns of precipitation intensity as observed by the NAME Event Rain Gauge Network from 2002 to 2004. *J. Climate*, **20**, 1734–1750.
- Goddard, J. W. F., J. Tan, and M. Thurai, 1994: Technique for calibration of meteorological radars using differential phase. *Electron. Lett.*, **30**, 166–167.
- Higgins, W., and Coauthors, 2006: The NAME 2004 field campaign and modeling strategy. *Bull. Amer. Meteor. Soc.*, **87**, 79–94.
- Hitschfeld, W. F., and J. Bordan, 1954: Errors inherent in the radar measurement of rainfall at attenuating wavelengths. *J. Meteor.*, **11**, 58–67.
- Iguchi, T., T. Kozu, R. Meneghini, J. Awaka, and K. Okamoto, 2000: Rain-profiling algorithm for the TRMM Precipitation Radar. *J. Appl. Meteor.*, **39**, 2038–2052.
- Joss, J., and R. Lee, 1995: The application of radar-gauge comparisons to operational precipitation profile corrections. *J. Appl. Meteor.*, **34**, 2612–2630.
- Kucera, P. A., W. F. Krajewski, and C. B. Young, 2004: Radar beam occultation studies using GIS and DEM technology: An example study of Guam. *J. Atmos. Oceanic Technol.*, **21**, 995–1006.
- Lang, T. J., D. A. Ahijevych, S. W. Nesbitt, R. E. Carbone, S. A. Rutledge, and R. Cifelli, 2007: Radar-observed characteristics of precipitating systems during NAME 2004. *J. Climate*, **20**, 1713–1733.
- Nesbitt, S. W., D. Gochis, and T. J. Lang, 2008: The diurnal cycle of clouds and precipitation along the Sierra Madre Occidental observed during NAME-2004: Implications for warm season precipitation estimation in complex terrain. *J. Hydrometeorol.*, **9**, 728–743.
- Pellarin, T., G. Delrieu, G.-M. Saulnier, H. Andrieu, B. Vignal, and J.-D. Creutin, 2002: Hydrologic visibility of weather radar systems operating in mountainous regions: Case study for the Ardeche catchment (France). *J. Hydrometeorol.*, **3**, 539–555.

- Rowe, A. K., S. A. Rutledge, T. J. Lang, P. E. Ciesielski, and S. M. Saleeby, 2008: Elevation-dependent trends in precipitating features observed by the NAME radar network. *Mon. Wea. Rev.*, **136**, 4962–4979.
- Ryzhkov, A. V., and D. S. Zrnić, 1996: Assessment of rainfall measurement that uses specific differential phase. *J. Appl. Meteor.*, **35**, 2080–2090.
- , S. E. Giangrande, V. M. Melnikov, and T. J. Schuur, 2005: Calibration issues of dual-polarization radar measurements. *J. Atmos. Oceanic Technol.*, **22**, 1138–1155.
- Sarchilli, G., E. Gorgucci, V. Chandrasekar, and A. Dobaie, 1996: Self-consistency of polarization diversity measurement of rainfall. *IEEE Trans. Geosci. Remote Sens.*, **34**, 22–26.
- Simpson, J. R., R. F. Adler, and G. R. North, 1988: A proposed Tropical Rainfall Measuring Mission (TRMM) satellite. *Bull. Amer. Meteor. Soc.*, **69**, 278–295.
- Tabary, P., 2007: The new French operational radar rainfall product. Part I: Methodology. *Wea. Forecasting*, **22**, 393–408.
- , J. Desplats, K. Do Khac, F. Eideliman, C. Gueguen, and J.-C. Heinrich, 2007: The new French operational radar rainfall product. Part II: Validation. *Wea. Forecasting*, **22**, 393–408.
- Tessendorf, S. A., L. J. Miller, K. C. Wiens, and S. A. Rutledge, 2005: The 29 June 2000 supercell observed during STEPS. Part I: Kinematics and microphysics. *J. Atmos. Sci.*, **62**, 4127–4150.
- Vivekanandan, J., D. N. Yates, and E. A. Brandes, 1999: The influence of terrain on rainfall estimates from radar reflectivity and specific propagation phase observations. *J. Atmos. Oceanic Technol.*, **16**, 837–845.
- Zrnić, D. S., and A. Ryzhkov, 1996: Advantages of rain measurements using specific differential phase. *J. Atmos. Oceanic Technol.*, **13**, 454–464.